Journal of Power Sources 195 (2010) 2638–2643

Contents lists available at ScienceDirect

Journal of Power Sources

journal homepage: www.elsevier.com/locate/jpowsour

Short communication

Promotion of the electrocatalytic activity of a bimetallic platinum–ruthenium catalyst by repetitive redox treatments for direct methanol fuel cell

Sheng-Yang Huang [a,*], Chuin-Tih Yeh [b]

[a] Center of Electrochemical Engineering, Department of Chemical Engineering, University of South Carolina, Columbia, SC 29208, USA
[b] Department of Chemical Engineering and Materials Science, Yuan Ze University, Chung-Li 32003, Taiwan, ROC

ARTICLE INFO

Article history:
Received 23 September 2009
Received in revised form
11 November 2009
Accepted 12 November 2009
Available online 18 November 2009

Keywords:
Fuel cells
Methanol oxidation reaction
Platinum–ruthenium catalyst
Redox chemistry
Crystalline ruthenium dioxide

ABSTRACT

Pt–Ru/C catalyst (12 wt%) was prepared by the incipient wetness impregnation method followed by a redox heat-treatment. Transmission electron microscopy (TEM) results revealed uniformly distributed metallic crystallites of Pt–Ru alloy nanoparticles ($d_{PtRu} = 2.1 \pm 1.0$ nm). The effect of redox treatments of the impregnated catalysts on methanol oxidation reaction (MOR) was examined by cyclic voltammetry (CV). The MOR activity of the PtRu/C was significantly improved after each oxidation step of the redox treatment cycles. The enhanced catalytic activity was found to be quite stable in chronoamperometry (CA) measurements. CV, X-ray photoelectron spectroscopy (XPS), and X-ray diffraction (XRD) results strongly suggested that the improved catalytic activity was due to the formation of a stable c-RuO_x ($x = 2$–3) domain during the oxidation treatments. A bifunctional based mechanism was proposed for the MOR on the oxidized PtRu/C catalysts. Formation of Ru–OH species on the surface of c-RuO_x domains was suggested as stale sites for the oxidation of carbon monoxide adsorbed on the Pt catalytic sites.

1. Introduction

Direct methanol fuel cells (DMFCs) use aqueous methanol solution as a fuel to produce electricity and have a potential application in mobile power-supply systems [1]. Supported platinum (Pt) and Pt-alloys have been extensively used as electrocatalysts for methanol oxidation reaction (MOR) [2,3]. However, the high cost and poor efficiency of the Pt based electrocatalysts restrain the commercialization of DMFCs [4–6]. Accordingly, a decrease in Pt loading is essential for the development of efficient and cost effective anode catalysts. Practical approaches include (1) decreasing the particle size (or increasing the number of catalytically active sites) of Pt electrocatalysts [7–10], (2) increasing the accessibility of catalytically active sites for methanol [11–13], and (3) improving the tolerance against CO poison [14].

During methanol oxidation at the anode, carbon monoxide (CO) is produced as an intermediate Eq. (1) which gets adsorbed on the active Pt sites and poisons its catalytic activity:

$$Pt + CH_3OH \rightarrow Pt\text{–}CO + 4H^+ + 4e^- \quad (1)$$

The adsorbed CO can be oxidized to poisonless CO_2 by water Eq. (2) at the cost of overpotential (η):

$$Pt\text{–}CO + H_2O \rightarrow Pt + CO_2 + 2H^+ + 2e^- \quad (2)$$

The η required for the CO oxidation depends substantially on the nature of the electrocatalysts used [15,16]. For monometallic Pt catalysts, a high $\eta \approx 0.6$ V is generally needed. The state-of-the-art MOR electrocatalyst design relies on bimetallic catalysts [17,18]. In Pt based catalysts, ruthenium (Ru) has been extensively explored as the best promoting component. MOR catalysts consisting of Pt and Ru with compositions ranging from Pt_{30}–Ru_{70} to Pt_{100}–Ru_0 (where the subscripts indicate the respective atomic percentages) [19] have been synthesized and were finely dispersed as alloy crystallites on active carbon. Generally, bimetallic catalysts with an average crystallite size of $d \leq 3$ nm are used as DMFC anode [1,6]. Furthermore, Pt–Ru bimetallic catalysts facilitated reduction in η required for the CO oxidation (<0.3 V). The role of Ru on the suppression of CO poison has been attributed to two reasons, namely, bifunctional effect [20] and electronic effect [21].

Rolison et al. [22] emphasized the importance of hydrous ruthenium oxide because of the $RuO_2 \cdot xH_2O$ speciation present in the PtRu black catalyst, which enhances both electron and proton conductivities, resulting in a much more active catalyst for MOR. Recently, Qiu and co-workers [5] reported that the Pt/$RuO_2 \cdot xH_2O$/CNT catalyst prepared by multistep deposition exhibited excellent performance for MOR. In this work, we report the synthesis of a 12 wt% PtRu/C electrocatalyst and its electrocatalytic activity with respect to repetitive redox heat-treatments (reduction under hydrogen atmosphere at $T_r = 350\,^\circ$C and oxidation in air at $T_o = 250\,^\circ$C). The electrocatalytic activities of the PtRu/C for MOR are compared after each heat-treatment step. In addition, we also report our experience on the reversibility between

* Corresponding author. Tel.: +1 803 777 7314; fax: +1 803 777 8265.
E-mail address: huangs@cec.sc.edu (S.-Y. Huang).

0378-7753/$ – see front matter © 2009 Elsevier B.V. All rights reserved.
doi:10.1016/j.jpowsour.2009.11.049

Table 1
chemical and physical characteristics of Red_m and Ox_m electrocatalysts.

Catalyst	d[a] (nm)	Species[b]	E_p[c] (V)	I_p[d] (mA cm^{-2})	I_{05}[e] (mA cm^{-2})
Red_1	2.1	PtRu	0.97	30.0	2.6
Ox_1	2.2	Pt, RuO_x	1.02	52.2	5.4
Red_2	2.3	Pt, PtRu, Ru	1.00	31.1	2.7
Ox_2	2.4	Pt, Ru, RuO_x	1.05	53.2	5.5
Red_3	–	Pt, PtRu, Ru	1.03	32.3	2.7
Ox_3	–	Pt, Ru, RuO_x	1.04	53.2	5.6

[a] Nominal diameter of alloy crystallites estimated from TEM.
[b] Species found by XRD.
[c] Peak potential.
[d] Peak current density.
[e] Current density at 0.5 V.

Ru and RuO_x during repetitive redox treatments and on the activity and stability of c-RuO_x phase formed during the oxidation treatments.

2. Experimental

2.1. Catalyst preparation

12 wt% PtRu/C (8 wt% Pt and 4 wt% Ru, with an intended atomic ratio of Pt–Ru at 1:1) bimetallic electrocatalyst was prepared by the incipient wetness impregnation method using Vulcan XC-72R carbon as support. Elemental analysis (measured by ICP-AES) indicated metal contents of 7.4 wt% Pt and 3.7 wt% Ru on the prepared electrocatalyst. Then, the catalyst was subsequently subjected to repetitive redox heat-treatments. The heat-treated catalysts were marked as Red_m or Ox_m, in which Red and Ox denote the type (reduction or oxidation) of their final heat-treatment while the subscript m represents the number of repetitive heat-treatments. For example, Red_1 electrocatalyst was obtained by the reduction of freshly impregnated catalyst while Ox_2 catalyst was obtained by the oxidation of Red_2. Table 1 lists the chemical and physical properties of the electrocatalysts obtained after such redox treatments.

2.2. Catalyst characterization

The physical properties of the heat-treated catalysts were characterized by inductively coupled plasma-atomic emission spectrometry (ICP-AES), X-ray diffraction (XRD), transmission electron microscopy (TEM), and X-ray photoelectron spectroscopy (XPS). High-resolution XRD studies were conducted at beamline BL17C of National Synchrotron Radiation Research Center (NSRRC) at Hsinchu, Taiwan, using an X-ray line with λ = 0.99988 Å. Diffraction signals were accumulated for 10 min and recorded by an imaging plate positioned 29.5 cm away from the sample. TEM was performed using a JEOL-2010 microscope equipped with a LaB_6 electron gun and operated at 200 kV. A ULVAC-PHI Quantera SXM spectrometer with an Al K_α monochromatic source (15 kV, 20 mV) was used for the XPS analysis. The binding energy scale was calibrated using the C_{1s} (284.5 eV) signal. The XPSPEAK software Version 4.1 was used and the spectral peaks were fitted using a mixed Gaussian–Lorentzian line shape and Shirley baselines. Linearity of the BE scale of the detector was assured using four Au peaks, namely Au($4f_{7/2}$) (84.0 eV), Au($4d_{5/2}$) (335.2 eV), Au($4p_{3/2}$) (546.4 eV) and Au(4s) (762.2 eV).

2.3. Electrochemical measurements

600B cyclic-voltammeter (CV) (CH Instruments) was used to characterize the electrocatalytic activity of the prepared electrocatalysts for MOR. A three electrode electrochemical cell comprising a working electrode, a platinum film counter electrode, and an Ag/AgCl reference electrode was used for all the electrochemical measurements. The electrolyte employed for the electrochemical studies was a mixture of 1.0 M CH_3OH and 0.5 M H_2SO_4. Catalyst ink for the studies was prepared by dispersing 10 mg of the catalyst powders (including the home-made catalysts and a commercial catalyst of 20 wt% PtRu/C from E-TEK) in 0.5 mL 2-propanol (from Fluka) for 30 min in an ultrasonic bath. The ink was then brushed onto a carbon paper (2 cm^2, ElectroChem EC-TP1-060) as catalyst for the working electrode. The total loading of the catalyst was maintained at 1.0 mg cm^{-2}. The MOR activity of the catalysts was studied by cycling the potential between 0.0 V and 1.2 V [vs RHE (reversible hydrogen electrode)] at a scan rate of 20 mV s^{-1} at room temperature. The electrolyte was purged with N_2 for 30 min prior to the electrochemical measurements and purging was continued throughout the experiment. The CV profiles reported in this study represented data from the 16th cycle in order to maintain similar reaction conditions for all the catalysts studied. After the CV scans, chronoamperometry (CA) was also performed with same catalysts for 3600 s at constant potential (0.5 V vs RHE).

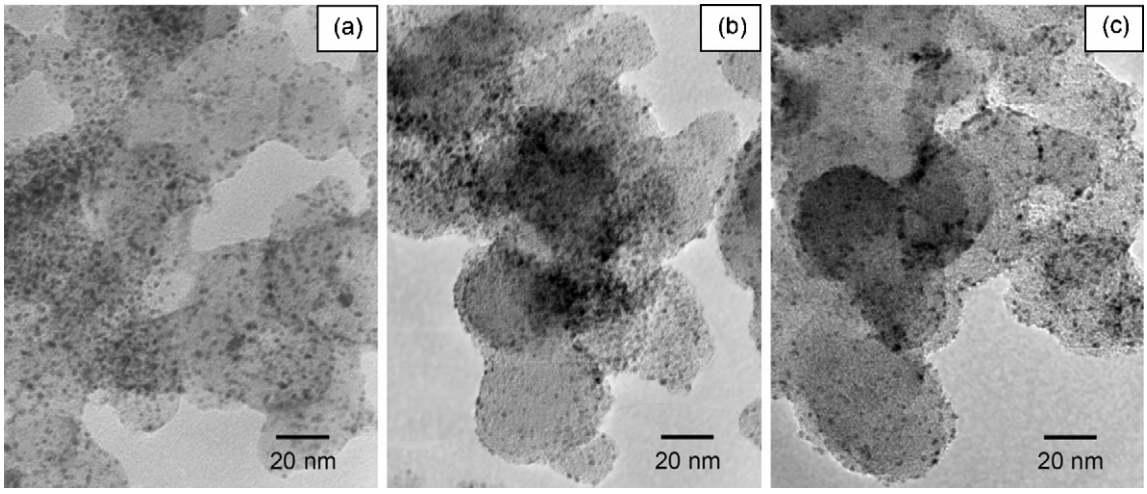

Fig. 1. TEM micrographs of PtRu/C electrocatalysts: (a) Red_1; (b) Ox_1; and (c) Red_2. The average size of PtRu alloy particle was d_{PtRu} = (a) 2.1 nm, (b) 2.2 nm, and (c) 2.3 nm.

3. Results and discussion

3.1. TEM and XRD characterization

Fig. 1 compares the transmission electron micrographs of Red_1, Ox_1, and Red_2 electrocatalysts. The catalyst particles (Fig. 1a) were uniformly deposited on the carbon support (Vulcan XC-72R, with a diameter ~50 nm). An average particle size of $d_{PtRu} = 2.1 \pm 1.0$ nm was obtained based on randomly picked 300 particles. Similar d_{PtRu} was found in Ox_1 (2.2 nm, Fig. 1b) and Red_2 (2.3 nm, Fig. 1c) catalysts. In addition, the TEM results indicated that the Pt–Ru crystallites exhibited good resistance to particle growth during the repetitive redox treatments.

Fig. 2 compares the XRD patterns of Red_m and Ox_m electrocatalysts. For the Red_1 catalyst, two major diffraction peaks were noticed at $2\theta = 25.7$ and 29.8° which represented the (1 1 1) and (2 0 0) diffractions of Pt–Ru alloy nanocrystallites. The XRD results revealed that the Ru atoms in Red_1 catalyst have alloyed with the fcc crystallites of Pt since no diffraction peak was observed for the hexagonal Ru. A slight decrease in the lattice parameter from 3.923 to 3.855 Å also confirmed that Ru atom was incorporated into the fcc phase. The peak width of Pt–Ru (1 1 1), according to the Debye–Scherrer equation, suggested that the alloy particles of the Red_1 catalyst had an average size of $d_{PtRu} = 2.3$ nm, which is in good agreement with 2.1 nm calculated from TEM image shown in Fig. 1. The intensity of Pt–Ru alloy peaks of the Red_1 catalyst diminished and new peaks were noticed at $2\theta = 18.1$, 22.6, and 34.5° for the Ox_1 catalyst. These new peaks were assigned to the diffraction of (1 1 0), (1 0 1), and (2 1 1) planes of c-RuO_2 (crystalline ruthenium dioxide) obtained from the following oxidation reaction at $T_o = 250$ °C:

$$Ru + O_2 \rightarrow \text{c-}RuO_2 \quad (3)$$

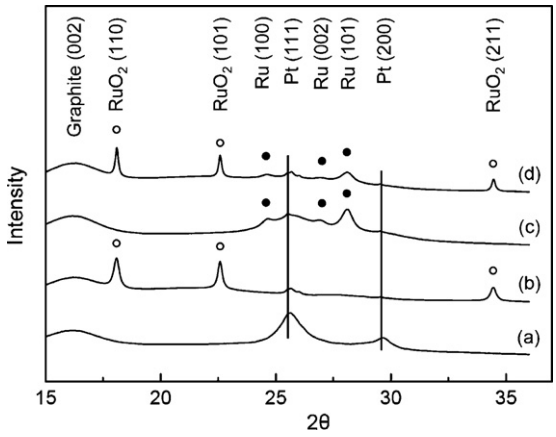

Fig. 2. XRD patterns (X-ray wavelength of 0.99988 Å) of PtRu/C electrocatalysts: (a) Red_1; (b) Ox_1; (c) Red_2; and (d) Ox_2. The average size of dispersed PtRu alloy particles estimated from Pt (1 1 1) in the Red_1 catalyst was $d_{PtRu} = 2.3$ nm. The Red_1, Red_2, and standard Pt showed a lattice parameter of 3.855, 3.910, and 3.923 Å, respectively.

Composite diffractions arising from the weak fcc Pt–Ru peaks and strong hexagonal Ru peaks were found in Red_2 catalyst (Fig. 2c). In addition, metallic Ru was also formed by the reduction of c-RuO_2 Eq. (4):

$$\text{c-}RuO_2 + 2H_2 \rightarrow Ru + 2H_2O \quad (4)$$

The presence of prominent peaks of monometallic Ru in the XRD pattern of Red_2 strongly suggested an irreversible segregation of Ru from Pt–Ru alloy during the oxidation treatment of Ox_1. Conversely, the weak diffraction peaks of hexagonal Ru remained in the Ox_2 (Fig. 2d) after the re-oxidation treatment of Red_2. The XRD analysis of Ox_2 catalyst suggested that a fraction of

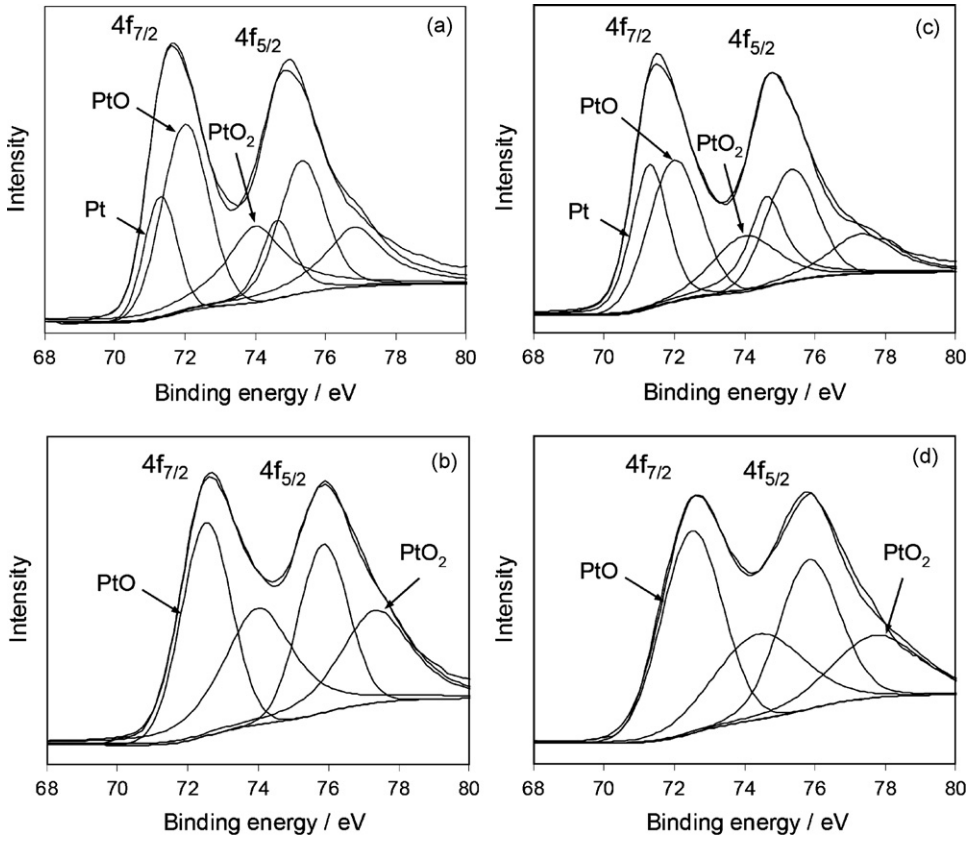

Fig. 3. X-ray photoelectron spectra of Red_m and Ox_m electrocatalysts from Pt(4f): (a) Red_1; (b) Ox_1; (c) Red_2; and (d) Ox_2.

Ru was retained in the metallic state during the oxidation of Red_2 to Ox_2.

3.2. XPS characterization

Pantea et al. [23] reported that Vulcan XC-72R contains 0.5 at.% of sulfur on the graphene layer surface. It is well-known that sulfur atoms react readily with Pt to form PtS species that may poison the active Pt sites. However, no sulfur atoms were detected on Red_1 catalyst from the XPS survey scan which revealed that a major fraction of sulfur atoms on the fresh catalyst had been removed during the reduction pretreatment. Furthermore, the signal for C_{1s} at 284.5 eV from the carbon support overlapped to that of $Ru(3d_{3/2})$ (284.3 eV) and prevented the detailed examination of Ru species using this peak [24].

Fig. 3 exhibits detailed Pt(4f) spectra of Red_m and Ox_m catalysts. As can be seen, each spectrum was composed of doublet peaks of $4f_{7/2}$ (71.5–72.6 eV) and $4f_{5/2}$ (74.8–75.9 eV) with the theoretical peak area ratio of 4:3. Column 2 in Table 2 summarizes the effects of repetitive redox treatments on the chemical shift of $Pt(4f_{7/2})$. A comparison with the binding energies (BEs) of standard Pt^0 samples (71.0 eV) indicated that the Pt in Red_m existed mainly in a slightly oxidized state. The fitting results of Red_m in Table 3 also confirmed that the major component in Red_m catalyst was platinum oxide (PtO).

Park et al. [21] observed a decrease in the BEs of $Pt(4f_{7/2})$ to less than 71.0 eV when alloying Ru with Pt. An electron transfer from Ru to Pt within the Pt–Ru alloy was thus suggested. The electron transfer significantly reduced the Pt–CO bond strength which might have lowered the η required for methanol decomposition at the anode. Therefore, an electronic effect was proposed for the function of Ru towards MOR in the PtRu bimetallic catalysts. In our XPS studies, the BE of $Pt(4f_{7/2})$ peaks of the Red_m catalysts shown in Table 2 were always lower than those for the Ox_m catalysts. However, the $Pt(4f_{7/2})$ peaks of Red_m electrocatalysts showed a slightly higher BE than the metallic Pt (71.0 eV). The observed shift of $Pt(4f_{7/2})$ may be attributed to the oxidation of surface platinum atoms (Pt^s) to Pt^sO_x ($x = 1–2$) during the catalyst manipulation when subjecting

Table 2
XPS analysis: effect of repetitive redox treatments on the binding energy of $Pt(4f_{7/2})$ and $Ru(3p_{3/2}$ for Red_m and Ox_m electrocatalysts.

Catalyst	$Pt(4f_{7/2})$ (eV)	$Ru(2p_{3/2})$ (eV)
Red_1	71.6	462.5
Ox_1	72.6	463.4
Red_2	71.5	462.1
Ox_2	72.6	463.0
Pure Pt	71.0	–
PtO	72.5	–
PtO_2	74.0	–
Pure Ru	–	462.0
RuO_2	–	463.4
RuO_3	–	466.9

Table 3
XPS analysis: chemical states and peak area ratios of Red_m and Ox_m electrocatalysts.

Chemical state	XPS area ratio (%)			
	Red_1	Ox_1	Red_2	Ox_2
Pt	20.6	0	33.7	0
PtO	45.1	50.1	42.1	59.9
PtO_2	34.3	49.9	24.2	40.1
Ru	62.9	13.4	77.2	22.0
RuO_2	14.2	72.1	11.8	56.9
RuO_3	22.9	14.5	11.0	21.1

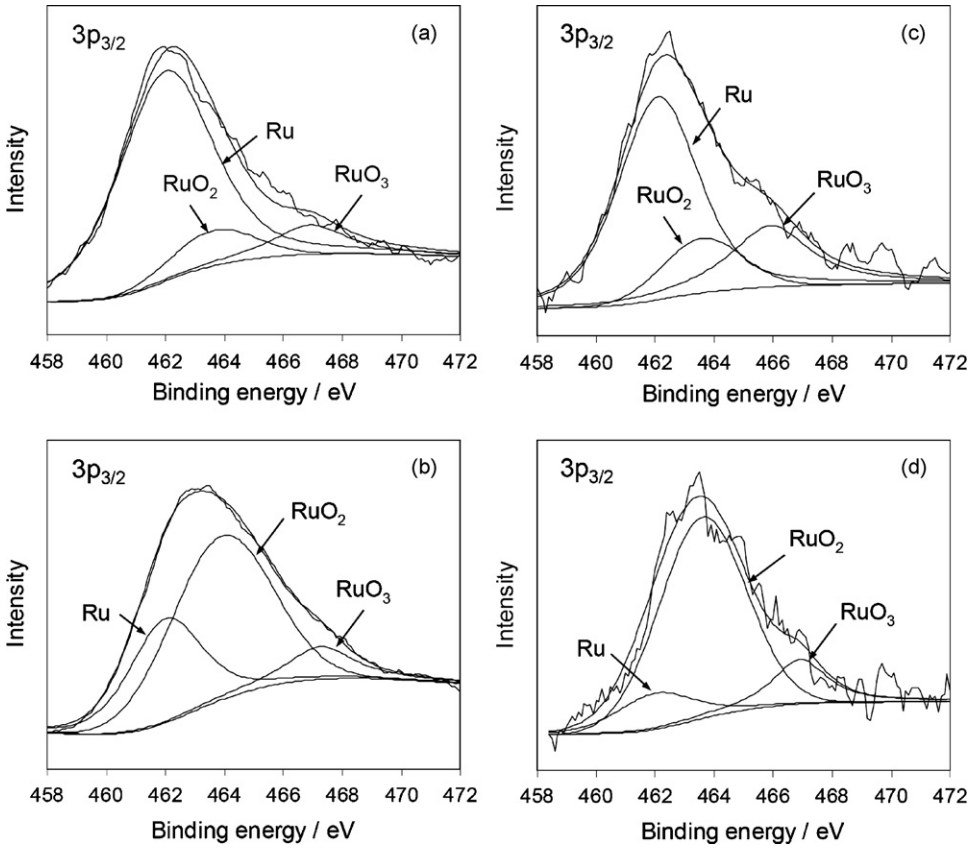

Fig. 4. X-ray photoelectron spectra of Red_m and Ox_m electrocatalysts from $Ru(3p_{3/2})$: (a) Red_1; (b) Ox_1; (c) Red_2; and (d) Ox_2.

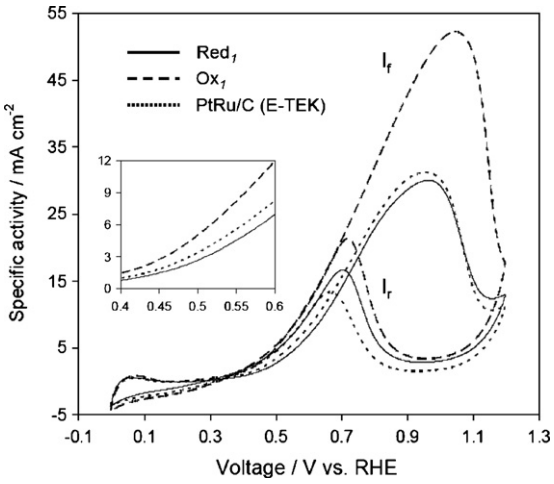

Fig. 5. Cyclic voltammograms of MOR on reduced (Red_1) and oxidized (Ox_1) PtRu/C electrocatalysts in 1.0 M methanol/0.5 M H_2SO_4 at a scan rate of 20 mV s^{-1}.

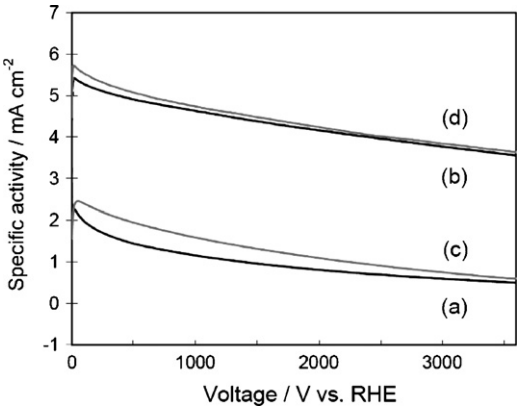

Fig. 6. Chronoamperometry curves for the MOR of different PtRu/C electrocatalysts: (a) Red_1, (b) Ox_1, (c) Red_2, and (d) Ox_2 in 1.0 M CH_3OH and 0.5 M H_2SO_4 electrolyte at 0.5 V (vs RHE) at the room temperature.

the catalysts to redox heat-treatments:

$$2Pt^s + xO_2 \rightarrow 2Pt^sO_x \quad (5)$$

Since the Ru(3d) signal was affected by the C_{1s} signal, the chemical state of Ru was investigated by using the Ru(3p) peak. Fig. 4 exhibits detailed Ru($3p_{3/2}$) spectra of Red_m and Ox_m catalysts. The broad Ru($3p_{3/2}$) peak found in all of the treated catalysts can be attributed to a combined contribution from the three oxidation states of Ru (Ru^0, RuO_2 and RuO_3). Column 3 in Table 2 summarizes the effects of repetitive redox treatments on the maximum of Ru($3p_{3/2}$) peaks of Red_m and Ox_m electrocatalysts. The Ox_m and Red_m catalysts showed different peak maximums at 463.4 and 462.1 eV, respectively. For Red_1, the composition was 77.2% metallic ruthenium and 22.8% ruthenium oxide (Table 3). In contrast, the composition of Ox_1 was 22.0% Ru and 78.0% ruthenium oxide.

It is noteworthy from the XPS analysis shown in Table 3 that both Red_2 and Ox_2 catalysts showed slightly higher metal contents than Red_1 and Ox_1 due to the repetitive redox treatments which increased the crystallization of Pt–Ru crystallites. The redox process made the oxidation of surface ruthenium atoms (Ru^s) to Ru^sO_x more difficult during the catalyst manipulation steps. For Ox_m catalyst, the change in BEs may be caused by the segregation of Ru from Pt–Ru crystallites during the oxidation treatment of Ox_1. Interestingly, the surface RuO_x acted as a passive layer and prevented further oxidation of the core Ru metal as indicated in the XRD results (Fig. 2d).

3.3. Electrochemical performance

Fig. 5 depicts the effects of oxidation treatment on the electrocatalytic activity of PtRu/C electrocatalysts for the MOR. An onset potential for methanol oxidation was noticed at E_o = 0.23 V (vs RHE) for both Red_1 and Ox_1 catalysts. The current density (I) for the Red_1 catalyst increased with the increase in the applied potential (E) and reached a peak current density (I_p) of 30 mA cm^{-2} at E_p = 0.97 V. Further increase in the potential resulted in decreased I, due to the loss of active Pt sites due to the formation of surface oxide species at high potentials. From Fig. 5 it can be seen that, the Ox_1 catalyst had a much higher electrocatalytic activity for the MOR than the Red_1 catalyst. The ratio of forward peak current density (I_f) to reverse peak current density (I_r) can be used to describe the catalyst's tolerance to the carbonaceous species accumulation [25]. A High I_f/I_r ratio indicated better oxidation of methanol to carbon dioxide during the anodic scan and less accumulation of carbonaceous residues on the Pt surface. The I_f/I_r ratio of 2.45 obtained for the Ox_1 catalyst was higher than that of Red_1 catalyst (I_f/I_r = 1.80), which indicated that more intermediate carbonaceous species were oxidized to carbon dioxide in the forward scan of Ox_1 than that of Red_1.

The last column in Table 1 summarizes the variation of I_{05} (current density at an applied potential of 0.5 V vs RHE) for the Red_m and Ox_m catalysts during the MOR. The reduced catalysts (Red_1, Red_2, and Red_3) generally showed low I_{05} values of approximately 2.7 mA cm^{-2}. A drastic increase in the I_{05} value to 5.5 mA cm^{-2} was noticed for the catalysts oxidized at T_o = 250 °C (Ox_1, Ox_2, and Ox_3) which suggested that the Ox_m catalysts were remarkably more active than the Red_m catalysts. From the XPS and XRD results, the observed increase in the I_{05} value for the Ox_m catalysts can be attributed to the speciation of c-RuO_x (x = 2–3) during oxidation treatments.

Fig. 6 compares the chronoamperometry results of Red_m and Ox_m during the MOR. The value of I_{05} gradually decreased over time for all the electrocatalysts tested. Noticeably, Ox_m and Red_m electrocatalysts displayed similar decay rates. The observed decay was attributed to the accumulation of intermediate species, such as $-CO_{ad}$, $-CHO_{ad}$, and $-CH_3OH_{ad}$ [26,27], which were formed during the methanol oxidation on the catalyst particles. Interestingly, the initial current was resumed (not shown in the figure) after purging the electrolyte with N_2 for 30 min which indicated a certain degree of reversibility of catalytic activity. Furthermore, Ox_m catalysts were able to maintain a high I_{05} over 3600 s.

3.4. Correlation of I_{07} with the existence of c-RuO_2

The results obtained from Figs. 2, 4, and 6 strongly suggested that the high electrocatalytic activity of Ox_m was due to the formation of c-RuO_x domain during the oxidation treatment at T_o = 250 °C. It was therefore our hypothesis that the c-RuO_x present in the Pt–Ru catalyst was an excellent promoter for removing the poisonous CO. Watanabe and Motoo [20] proposed a bifunctional mechanism in which Ru is a promoting center for the generation of Ru–OH species and subsequent electrooxidation of poisoning CO into CO_2:

$$Ru + H_2O \rightarrow Ru\text{–}OH + H^+ + e^- \quad (6)$$

$$Pt\text{–}CO + Ru\text{–}OH \rightarrow Pt + Ru + CO_2 + H^+ + e^- \quad (7)$$

Similarly, the promotion of the catalysts synthesized in this study could be described by the following bifunctional-like mechanism occurred on the perimeter of Pt and c-RuO_x:

$$c\text{-}RuO_x + H_2O \rightarrow RuO_{x-1}(OH)_2 \quad (8)$$

$$RuO_{x-1}(OH)_2 + Pt\text{–}CO \rightarrow c\text{-}RuO_x + Pt + CO_2 + 2H^+ + 2e^- \quad (9)$$

Recently, Dmowski et al. [28] reported that ruthenium dioxide adsorbs (chemisorb and physisorb) water under humidified environments to form nonstoichiometric hydrated ruthenium oxide ($RuO_2{\cdot}yH_2O$). Kreuer et al. [29,30] have also reported that RuO_2 can efficiently dissociate H_2O to form surface hydroxyl groups. Hence, we postulated that the water molecules adsorbed on c-RuO_x (x = 2–3) were able to convert RuO_x surface into hydroxide groups Eq. (10).

$$c\text{-}RuO_x{\cdot}yH_2O \leftrightarrow c\text{-}RuO_{x-y}(OH)_{2y} \quad (10)$$

Conceivably, the c-RuO_x structure of Ox_m catalyst can supply stable Ru–OH species which was active for removing strongly adsorbed CO via Eq. (9) during MOR.

Hydrous ruthenium oxide has been reported as a mixed electronic–protonic conductor [31,32]. The low mass transport characteristics and high electronic conductivity of c-$RuO_x{\cdot}yH_2O$ offer a promotional effect to the Pt–Ru catalysts during MOR. Therefore, the marked increase in activity of Ox_m obtained through the oxidation treatment of Red_m was attributed to the oxidation of Ru into active c-RuO_x phase.

4. Conclusions

In this study, 12 wt% Pt–Ru/C electrocatalyst was synthesized and the effect of redox treatments on the electrochemical activity for MOR was studied. The following conclusions have been deduced:

1. Oxidized PtRu/C electrocatalysts (Ox_m) had remarkably higher catalytic activity towards MOR than the reduced electrocatalysts (Red_m).
2. The promotion of oxidation treatment at T_o = 250 °C was attributed to the formation of c-RuO_x (x = 2–3) phase.
3. The mechanism of c-RuO_x promotion involves the formation of Ru–OH species on the surface (bifunctional based mechanism).
4. The promotion effect can last for quite a longer period because the c-RuO_x phase was stable during the electrooxidation reaction.

Acknowledgements

Financial support from National Science Council and the Educational Ministry of the Republic of China is gratefully acknowledged. We would also like to thank the comments from Dr. Prabhu Ganesan of the University of South Carolina.

References

[1] M.P. Hogarth, T.R. Ralph, Platinum Met. Rev. 46 (2002) 146–164.
[2] S.Y. Huang, C.M. Chang, K.W. Wang, C.T. Yeh, Chemphyschem 8 (2007) 1774–1777.
[3] S.Y. Huang, S.M. Chang, C.T. Yeh, J. Phys. Chem. B 110 (2006) 234–239.
[4] S. Liao, K.-A. Holmes, H. Tsaprailis, V.I. Birss, J. Am. Chem. Soc. 128 (2006) 3504–3505.
[5] L. Cao, F. Scheiba, C. Roth, F. Schweiger, C. Cremers, U. Stimming, H. Fuess, L. Chen, W. Zhu, X. Qiu, Angew. Chem. Int. Ed. 45 (2006) 5315–5319.
[6] H.S. Liu, C.J. Song, L. Zhang, J.J. Zhang, H.J. Wang, D.P. Wilkinson, J. Power Sources 155 (2006) 95–110.
[7] H.P. Liang, H.M. Zhang, J.S. Hu, Y.G. Guo, L.J. Wan, C.L. Bai, Angew. Chem. Int. Ed. 43 (2004) 1540–1543.
[8] K.W. Wang, S.Y. Huang, C.T. Yeh, J. Phys. Chem. C 111 (2007) 5096–5100.
[9] D. Zhao, B.Q. Xu, Angew. Chem. Int. Ed. 45 (2006) 4955–4959.
[10] T. Matsumoto, T. Komatsu, K. Arai, T. Yamazaki, M. Kijima, H. Shimizu, Y. Takasawa, J. Nakamura, Chem. Commun. (2004) 840–841.
[11] M. Arenz, K.J.J. Mayrhofer, V. Stamenkovic, B.B. Blizanac, T. Tomoyuki, P.N. Ross, N.M. Markovic, J. Am. Chem. Soc. 127 (2005) 6819–6829.
[12] D.R. Rolison, Science 299 (2003) 1698–1701.
[13] H. Yang, Y. Yang, S.Z. Zou, J. Phys. Chem. B 110 (2006) 17296–17301.
[14] C. Roth, N. Benker, T. Buhrmester, M. Mazurek, M. Loster, H. Fuess, D.C. Koningsberger, D.E. Ramaker, J. Am. Chem. Soc. 127 (2005) 14607–14615.
[15] M.P. Hogarth, T.R. Ralph, Platinum Met. Rev 46 (2002) 117–135.
[16] S.Y. Huang, C.M. Chang, C.T. Yeh, J. Catal. 241 (2006) 400–406.
[17] H. Yano, C. Ono, H. Shiroishi, T. Okada, Chem. Commun. (2005) 1212–1214.
[18] E.S. Steigerwalt, G.A. Deluga, D.E. Cliffel, C.M. Lukehart, J. Phys. Chem. B 105 (2001) 8097–8101.
[19] A.S. Arico, P.L. Antonucci, E. Modica, V. Baglio, H. Kim, V. Antonucci, Electrochim. Acta 47 (2002) 3723–3732.
[20] M. Watanabe, S. Motoo, J. Electroanal. Chem. 60 (1975) 267–273.
[21] K.-W. Park, J.-H. Choi, S.A. Lee, C. Pak, H. Chang, Y.-E. Sung, J. Catal. 224 (2004) 236–242.
[22] J.W. Long, R.M. Stround, K.E. Swider-Lyons, D.R. Rolison, J. Phys. Chem. B 104 (2000) 9772–9776.
[23] D. Pantea, H. Darmstadt, S. Kaliaguine, L. Summchen, C. Roy, Carbon 39 (2001) 1147–1158.
[24] J. Chastain, Handbook of X-ray Photoelectron Spectroscopy, Perkin-Elmer Corporation, Eden Prairie, 1992.
[25] G.Y. Zhao, H.L. Li, Appl. Surf. Sci. 254 (2008) 3232–3235.
[26] J.W. Guo, T.S. Zhao, J. Prabhuram, R. Chen, C.W. Wong, J. Power Sources 156 (2006) 345–354.
[27] H. Hoster, T. Iwasita, H. Baumgartner, W. Vielstich, Phys. Chem. Chem. Phys. 3 (2001) 337–346.
[28] W. Dmowski, T. Egami, K.E. Swider-Lyons, C.T. Love, D.R. Rolison, J. Phys. Chem. B 106 (2002) 12677–12683.
[29] K.D. Kreuer, Chem. Mater. 8 (1996) 610–641.
[30] H. Over, Y.D. Kim, A.P. Seitsonen, S. Wendt, E. Lundgren, M. Schmid, P. Varga, A. Morgante, G. Ertl, Science 287 (2000) 1474–1476.
[31] E. Ticianelli, J.G. Beery, M.T. Paffett, S. Gottesfeld, J. Electroanal. Chem. 258 (1989) 61–77.
[32] K.E. Swider, C.I. Merzbacher, P.L. Hagans, D.R. Rolison, Chem. Mater. 9 (1997) 1248–1255.